5642 J. Med. Chem. 2009, 52, 5642–5648
DOI: 10.1021/jm9002457

Journal of Medicinal Chemistry Article

α-Tocopheryl Succinate as a Scaffold to Develop Potent Inhibitors of Breast Cancer Cell Adhesion

Dasheng Wang, Hsiao-Ching Chuang, Shu-Chuan Weng, Po-Hsien Huang, Hao-Yu Hsieh, Samuel K. Kulp, and Ching-Shih Chen*

Division of Medicinal Chemistry and Pharmacognosy, College of Pharmacy, The Ohio State University, 336 Parks Hall, 500 West 12th Avenue, Columbus, Ohio 43210

Received February 26, 2009

This study is aimed at the pharmacological exploitation of α-tocopheryl succinate (**1**) to develop potent antiadhesion agents. Considering the structural cooperativity between the phytyl chain and the carboxylic terminus in determining the antiadhesion activity, our structural optimization led to compound **5** ([2-(4,8-dimethyl-non-1-enyl)-2,5,7,8-tetramethyl-chroman-6-yloxy]-acetic acid), which exhibited an-order-of-magnitude higher potency than **1** in blocking the adhesion of 4T1 metastatic breast cancer cells to extracellular matrix proteins (IC_{50}, 0.6 μM versus 10 μM). Evidence indicates that the ability of compound **5** to block cell adhesion and migration was attributable to its effect on disrupting focal adhesion and actin cytoskeletal integrity by facilitating the degradation of focal adhesion kinase. Interactions between tumor cells and the ECM in the tumor microenvironment have been increasingly recognized as critical modulators of the metastatic potential of tumor cells. Consequently, the ability of compound **5** to block such interactions provides a unique pharmacological tool to shed light onto mechanisms that govern cell adhesion and tumor metastasis.

Introduction

The therapeutic potential of α-tocopheryl succinate (aka vitamin E succinate; **1**) in cancer treatment and prevention has been the focus of many recent investigations.[1,2] It is noteworthy that **1** suppresses in vitro and in vivo tumor cell growth without incurring significant toxicity to normal cells. A growing body of evidence indicates that **1** mediates its antitumor effect by perturbing a multitude of signaling pathways governing cancer cell growth, apoptosis, differentiation, angiogenesis, and metastasis. This broad spectrum of action in conjunction with low toxicity underlies the translational potential of **1** in cancer treatment or prevention. Of various target mechanisms reported in the literature, the inhibitory effect of **1** on cancer cell adhesion is especially noteworthy,[3] which is evident by the ability of α-tocopheryloxyacetic acid, a derivative with increased metabolic stability, to suppress breast tumor growth and to reduce lung metastasis in animal models.[4]

Substantial evidence indicates that adhesion is critical to the development of different aspects of the malignant phenotype of cancer cells, including survival, invasion, metastasis, and drug resistance.[5] Consequently, targeting adhesion or its associated pathways represents a therapeutically relevant strategy to improve the clinical outcome of many solid and hematological malignancies. Although humanized antibodies against different adhesion molecules have entered human trials,[6] there exist few small-molecule cell adhesion-targeted agents. Consequently, this study was aimed at the pharmacological exploitation of **1** to develop novel compounds with high potency in inhibiting cell adhesion. This structural optimization has led to a novel class of antiadhesion compounds with submicromolar potency.

Chemistry

We rationalized that the aliphatic side chain and the semisuccinate play a crucial role in mediating **1**'s antiadhesion activity. To assess the involvement of the phytyl side chain, we curtailed the chain length by the incremental removal of isopranyl units from the hydrophobic terminus, yielding **2** and **3** (Figure 1).

These truncated derivatives showed substantially improved potency vis-à-vis **1** in inhibiting the adhesion of 4T1 metastatic breast cancer cells to Matrigel-coated surface, with the relative potency of **2** > **3** > **1**. Moreover, increasing the rigidity of the side chain by introducing a double bond into **2**, resulting in compound **4**, gave rise to a multifold improvement in the antiadhesion potency. These findings underscore the pivotal role of the phytyl side chain in mediating the antiadhesion activity, of which two isopentyl units represented the optimal chain length.

We carried out further modifications of **2** and **4** by replacing the hemisuccinate with ether-linked C_2-C_5 carboxylic acids to generate two series of compounds (**I**: **5** and **7**−**9**; **II**: **6** and **10**−**12**), of which the rationale was 2-fold. First, like the phytyl side chain, the carboxylic function is also critically involved in ligand recognition by the target protein. Second, as the hemisuccinate is susceptible to enzymatic digestion, appendage of the carboxylic function through an ether linkage would increase the in vivo metabolic stability of the resulting derivatives. Of all these derivatives, **1** was derived from (*R*,*R*,*R*)-α-tocopherol while the others were synthesized from the chiral precursor (*S*)-6-hydroxy-2,5,7,8-tetramethylchroman-2-carboxylic acid methyl ester according to a general

*To whom correspondence should be addressed. Phone: (614)-688-4008. Fax: (614)-688-8556. E-mail: chen.844@osu.edu.

 Published on Web 08/26/2009

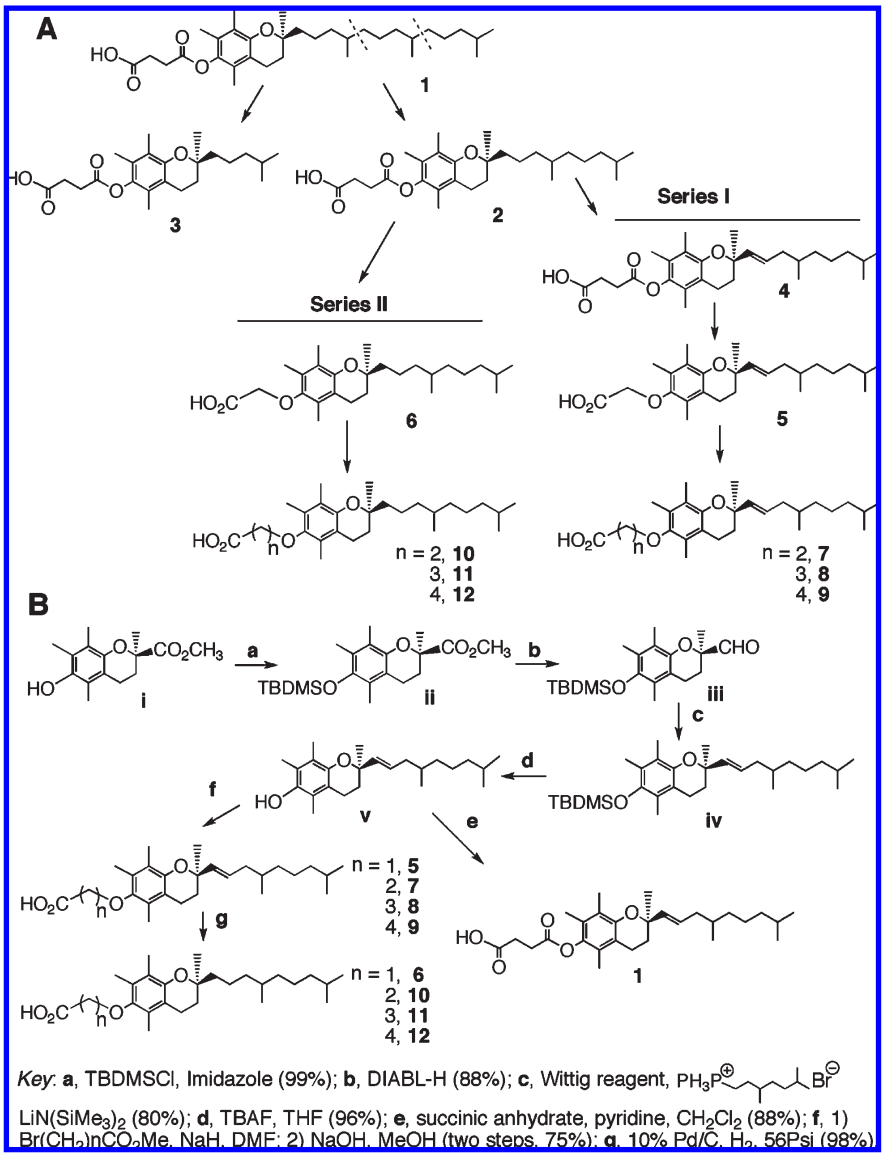

Figure 1. (A) Schematic representation of the course of structural optimization of compound **1** to develop antiadhesion agents. (B) General synthetic procedure for compound **1** derivatives.

procedure described in Figure 1B. However, all side chains used were racemic unless otherwise mentioned.

Results

Pharmacological Exploitation of 1 to Develop Potent Small-Molecule Inhibitors of Cell Adhesion. In this study, we used the 4T1 mouse mammary tumor cell line to investigate the antiadhesion activity of **1** and its derivatives because of the high propensity of 4T1 cells to metastasize to lung, liver, bone, and other sites,[7−9] a characteristic shared by stage IV human breast tumor cells. As shown, **1** exhibited a modest inhibitory effect on 4T1 cell adhesion to a Matrigel-coated surface (Figure 2B). While **1** inhibited 50% cell adhesion at 10 μM, its activity leveled off between 10 and 50 μM. Conceivably, this weak potency in conjunction with metabolic instability prohibited the clinical use of **1** in cancer therapy.

Although the molecular target by which **1** inhibited cell adhesion remains undefined, we hypothesized that the phytyl side chain and the succinate moiety were amenable to modifications to improve the antiadhesion potency of **1**. This premise was corroborated by the significantly improved potencies ($P < 0.01$) of **2** and, to a lesser extent, **3**, of which the alkyl side chains were shortened by one and two isopranyl units, respectively (Figure 2A).

The subsequent lead optimization of **2** was performed via two strategies: (1) inserting a double bond α-to the chromane ring to increase the rigidity of the side chain, and (2) replacing the hemisuccinate moiety with alkoxycarboxylic functions with varying chain lengths to increase metabolic stability. These modifications led to two series of derivatives, i.e., series I: compounds **4**, **5**, and **7**−**9**; series II: compounds **6**, and **10**−**12**. Many of these derivatives showed significantly improved activities relative to VES in inhibiting T41 cell adhesion ($P < 0.05$) (Figure 2A). Of them, compound **5** exhibited the highest potency, followed by compound **4**, with the respective IC_{50} values of 0.6 μM, and 1.3 μM vis-à-vis 2.5 μM for **2** (Figure 2B). Compound **5**, as distinguished by the α,β-unsaturated, truncated side chain and the ether-linked acetic acid, was three times more potent than its saturated counterpart, compound **6** (IC_{50}, 2 μM), underscoring the

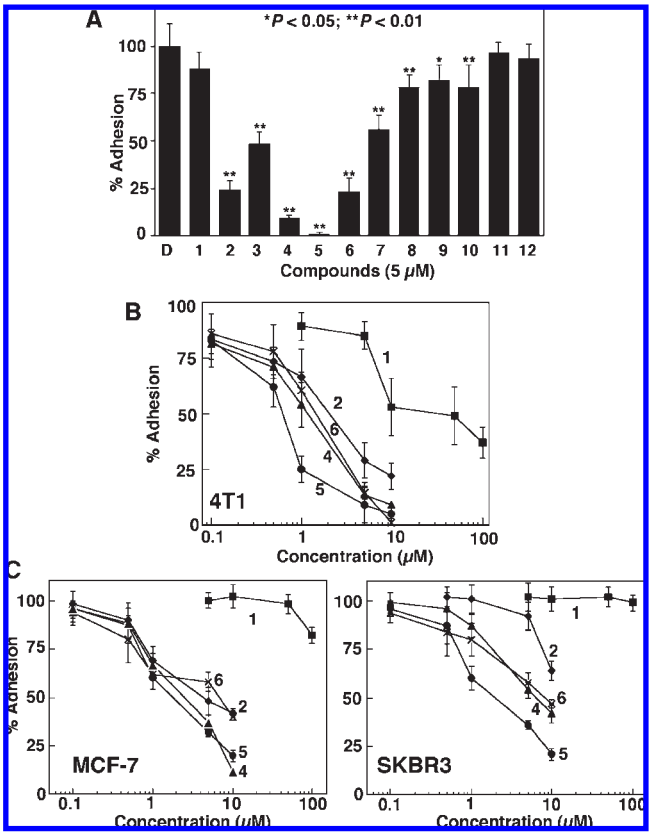

Figure 2. Suppression of breast cancer cell adhesion by compound **1** and its derivatives to a Matrigel-coated surface. (A) Effect of compound **1** and various derivatives, each at 5 μM, relative to DMSO (D) on the adhesion of 4T1 cells (*P < 0.05; **P < 0.01). Columns, mean; bars, SD (n = 3). (B) Dose-dependent effect of compounds **1**, **2**, and **4**−**6** on suppressing 4T1 cell adhesion. Points, mean; bars, SD (n = 3). (C) Dose-dependent effect of compounds **1**, **2**, and **4**−**6** on suppressing MCF-7 (left panel) and SKBR3 (right panel) cell adhesion. Points, mean; bars, SD (n = 3). Cell adhesion was analyzed as described in the Experimental Section.

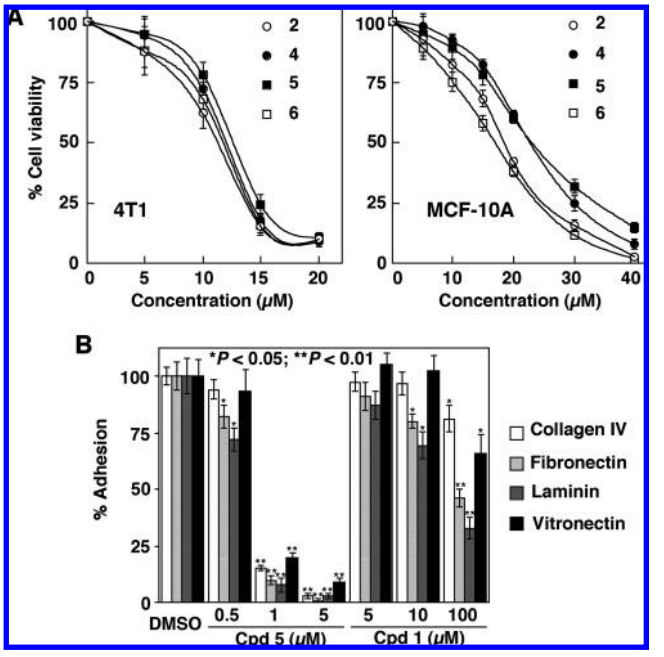

Figure 3. (A) Dose-dependent inhibitory effects of compounds **2** and **4**−**6** on the viability of 4T1 breast cancer cells (left pane) vs MCF-10A nonmalignant breast epithelial cells (right panel). 4T1 cells were treated with individual agents in 2% FBS-supplemented RPMI 1640 medium for 24 h, and cell viability after drug treatment was determined by the MTT assay as described in the Experimental Section. Points, mean; bars, SD (n = 6). (B) Does dependent effect of compound **5** vs compound **1** on suppressing 4T1 cell adhesion to the purified ECM proteins collagen IV, fibronectin, laminin, and vitronectin. Points, mean; bars, SD (n=3). Cell adhesion was analyzed as described in the Experimental Section. Statistical analysis was conducted relative to the DMSO control within in each ECM protein group (*P < 0.05; **P < 0.01).

importance of the rigidity of the alkyl chain in interacting with the target protein(s). Moreover, increases in the length of the alkoxy linker of **5** precipitously reduced the antiadhesion potency. Together, this finding indicates a subtle structure−activity relationship (SAR) in the effect of these derivatives on tumor cell adhesion.

Relative to 4T1 cells, noninvasive MCF-7 and SKBR3 breast cancer cells were also susceptible, although with less sensitivity, to the antiadhesion effect of these derivatives (Figure 2C). For example, the IC_{50} value of compound **5** for these two cell lines was approximately 2 μM, a 3.3-fold increase over that of 4T1, while **1** even at 100 μM was ineffective in suppressing the adhesion of these cells. This discrepancy might be related to differences in the metastatic potential among these cell lines.

Furthermore, we obtained evidence that the ability of these derivatives to block adhesion was not due to drug-induced cell death. Despite high potency in inhibiting cell adhesion, these optimal derivatives exhibited modest activities in suppressing 4T1 cell viability in 2% FBS, with IC_{50} values of greater than 10 μM (Figure 3A, left panel). As compared to 4T1 cells, MCF-10A nonmalignant breast epithelial cells exhibited a higher degree of resistance to the antiproliferative activity of these derivatives, with IC_{50} of 23 μM for compounds **4** and **5** (right panel).

On the basis of our finding, we rationalized that the antiadhesion effect of **1** and its derivatives was attributable to their abilities to interfere with the cellular interaction with extracellular matrix (ECM) proteins. As Matrigel, a partially defined ECM extract from mouse sarcoma, consists of a mixture of ECM components, we further investigated the effect of compound **5** vis-à-vis compound **1** on blocking the adherence of 4T1 cells to purified ECM proteins, including collagen IV, fibronectin, laminin, and vitronectin (Figure 3B). As shown, compound **5** at 0.5 μM and compound **1** at 5, 10, and 100 μM displayed differential activities in suppressing cell adhesion among these four ECM proteins, with the relative order of laminin > fibronectin > vitronectin, collagen IV. However, compound **5** at 1 μM or above could effectively suppress the adhesion to all of these ECM proteins (P < 0.01).

Inhibition of Migration and Lamellipodia Formation of 4T1 Metastatic Breast Tumor Cells. Pursuant to the above finding, we investigated the ability of the optimal compounds **2** and **4**−**6** vis-à-vis compound **1** to inhibit serum-induced 4T1 cell migration by using the Boyden chamber assay (Figure 4A). As shown, compounds **4**−**6** at 5 μM were effective in inhibiting cell migration in the order of **5** > **4** > **6**, in line with that of antiadhesion (P < 0.01). In contrast, compound **2** at 5 μM and VES even at 50 μM showed little effect.

To shed light onto the cellular basis for the inhibition of tumor cell migration by these derivatives, we investigated the effect of compound **1** (50 μM) versus compounds **5** (5 μM)

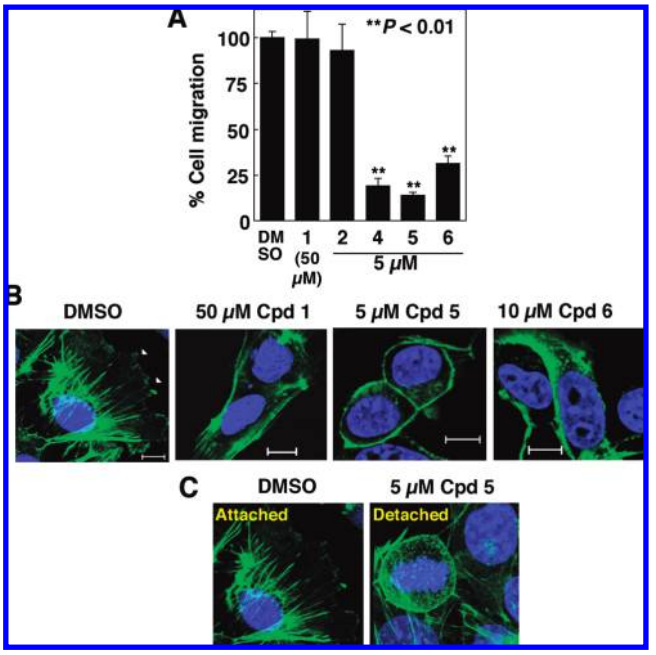

Figure 4. Compound **1** derivatives disrupt the migration and actin cytoskeletal structure of 4T1 cells. (A) Effects of compound **1** at 50 μM vs compounds **2** and **4**−**6**, each at 5 μM, on 4T1 cell migration. Cell motility was analyzed by the Transwell migration assay as described in the Experimental Section. Columns, mean; bars, SD (n = 3). (B) Immunocytochemical analysis of the effect of compounds **5** and **6** vs compound **1** on lamellipodia formation and actin stress fibers in 4T1 cells after 4 h of treatment. The arrows indicate lamellipodia formation. (C) The stacked 3-D analysis of the disruption of actin cytoskeletal structure by 5 μM compound **5**. The images show that cells with loss of stress fibers were rounded and detached from the surface (right panel), whereas actin filaments in the control cells (left panel) were intact and extended to the edge of the cell body and the cells were adhered to the surface.

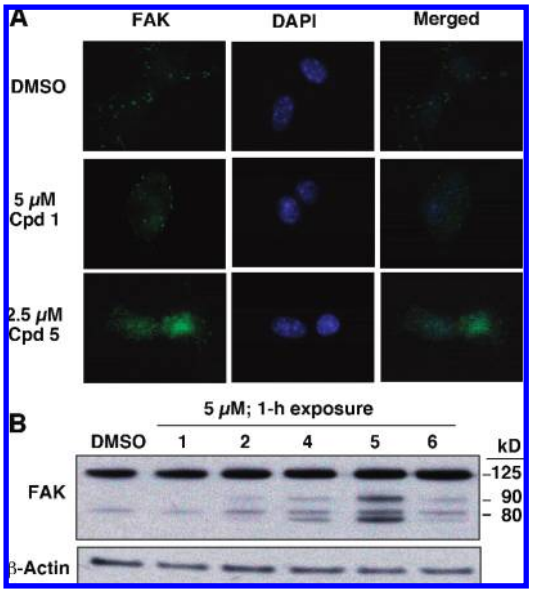

Figure 5. Effects of compound **1** vs compounds **2** and **4**−**6** on the expression of FAK, a central component of cell adhesion. (A) 4T1 cells were treated with 2.5 μM compound **5**, 5 μM compound **1** (negative control), or DMSO for 1 h, fixed, and immunostained with anti-FAK antibody. The distinct punctate staining pattern of FAK representing adhesive contacts at the cell periphery was evident in vehicle or compound **1** treated 4T1 cells but was no longer detectable following treatment with compound **5**. (B) 4T1 cells were treated with individual agents at the indicated concentration for 1 h, and cell lysates were immunoblotted with anti-FAK monoclonal antibody.

and **6** (10 μM) on the actin cytoskeleton in 4T1 cells by immunocytochemistry. After 4 h exposure, compounds **5** and **6** caused rapid dissolution of stress fiber and impairment of lamellipodia formation at the leading edge of 4T1 cells, while the actin stress fiber in compound **1** treated cells remained largely intact (Figure 4B). Quantitative analysis indicates that treatment of 4T1 cells with compounds **5** (5 μM) and **6** (10 μM) led to a reduction in the fluorescent intensity of F-actin by 84% and 70%, respectively, relative to the DMSO control (P < 0.01). Furthermore, the 3-D imagining of compound **5** treated cells showed detachment from neighboring cells or the surface of the culture dish as a result of stress fiber loss (Figure 4C). Similar to DMSO, cells treated with 50 μM compound **1** remained attached with intact actin cytoskeleton (data not shown). Moreover, we observed that treatment of 4T1 cells with compound **5** or **6** gave rise to the accumulation of small vesicles in areas surrounding the nucleus where the endoplasmic reticulum is typically located. The disintegration of the endoplasmic reticulum membrane might be associated with the drug-mediated loss of actin stress fibers.

Compound 1 Derivatives Target Focal Adhesion Kinase (FAK) Degradation. Considering the important role of FAK in regulating the formation of focal adhesions and actin stress fibers,[10,11] we assessed the effect of compound **5** (2.5 μM), with compound **1** (5 μM) as a negative control, on focal adhesion sites in 4T1 cells by immunostaining with anti-FAK antibodies (Figure 5A). As shown, while FAK staining displayed a typical punctate pattern representing the focal adhesion sites in the DMSO and compound **1** treated control cells, compound **5** treatment led to loss of focal adhesion sites, paralleling that of the aforementioned stress fiber dissolution (Figure 4B). It is noteworthy that the disruption of actin stress fibers and focal adhesion by compound **5** is reminiscent of that induced by mannitol in neuroblastoma cells.[12] As mannitol-induced cytoskeletal changes were preceded by the degradation of FAK, we investigated the effects of compound **5** relative to compounds **1**, **2**, **4**, and **6**, each at 5 μM, on FAK protein stability in 4T1 cells by Western blotting (Figure 5B). As shown, treatment with compound **5**, and to a lesser extent, **4** and **6**, induced FAK degradation, resulting in two major cleavage fragments with molecular masses of approximately 90 and 80 kDa. This degradation, however, was less evident or not appreciable in cells treated with compounds **1** and **2**, which paralleled the respective activities in blocking 4T1 cell adhesion.

Discussion

As cell adhesion has emerged as a promising therapeutic target in light of its critical role in promoting the invasive phenotype of cancer cells,[5] this study aimed at the pharmacological exploitation of compound **1** to develop potent antiadhesion agents. SAR analysis indicates that there exists a high degree of structural cooperativity between the phytyl side chain and the alkoxycarboxylic terminus of compound **1** in determining its antiadhesion activity. Among various derivatives examined, compound **5** represented the optimal agent with an-order-of-magnitude higher potency relative to compound **1** in blocking 4T1 cell adhesion (IC_{50}, 0.6 μM

versus 10 μM) and migration. Evidence indicates that the antiadhesion effect of compounds **1** and **5** was attributable to their ability to block cell adherence to EMC proteins. In contrast to 4T1 cells, MCF-7 and SKBR3 cells were less sensitive to the antiadhesion activity of compound **1** and its derivatives, suggesting a correlation with the invasiveness of these cell lines. Moreover, this high antiadhesion potency was independent of compound **5**'s cytotoxicity in 4T1 cells. The dissociation of these two pharmacological activities suggests a unique mode of mechanism underlying the strong activity of compound **5** in inhibiting cell adhesion.

We obtained evidence that the ability of compound **5** to block cell adhesion and migration was attributable to its effect on disrupting the formation of focal adhesion and actin cytoskeletal structures including lamellipodia and stress fibers through the stimulation of FAK degradation. This mode of action is reminiscent of that of mannitol-induced disruption of cytoskeletal structures, however, without the concurrent induction of apoptosis.[12] Thus, the mechanism by which compound **5** induces FAK degradation warrants further investigation given the importance of FAK signaling in mediating tumor angiogenesis and metastasis.[13] From a mechanistic perspective, compound **5** differs from other agents that target FAK proteolysis[14] or FAK kinase activity[15] and might provide a useful pharmacological probe to shed light onto the cellular regulation of FAK signaling and its role in facilitating tumor progression.

Conclusion

Cell adhesion represents an important therapeutic target not only in oncology but also in acute and chronic inflammatory diseases such as inflammatory bowel diseases[16] and autoimmune inflammation.[17] To date, most of the therapeutic development in targeting cell adhesion focuses on the blockade of integrin−ligand interactions by using monoclonal antibodies, antisense oligonucleotides, or small interference (si)RNAs, while very few small-molecule agents have been developed.[5] Our data indicate that the high potency of compound **5** in antiadhesion was attributable to its effect on interfering with cell adherence to ECM proteins, followed by FAK degradation. Interactions between tumor cells and the ECM in the tumor microenvironment have been increasingly recognized as critical modulators of the metastatic potential of tumor cells.[18] Consequently, the ability of compound **5** to block such interactions provides a unique pharmacological tool to shed light onto mechanisms that govern cell adhesion and tumor metastasis, which is currently under investigation.

Experimental Section

Chemical reagents and organic solvents were purchased from Sigma-Aldrich (St. Louis, MO) unless otherwise mentioned. Nuclear magnetic resonance spectra (^{1}H NMR) were measured on a Bruker DPX 300 model spectrometer. Chemical shifts (δ) were reported in parts per million (ppm) relative to the TMS peak. Electrospray ionization mass spectrometry analyses were performed with a Micromass Q-Tof II high-resolution electrospray mass spectrometer. The purity of all tested compounds are higher than 95% by elemental analyses, which were performed by Atlantic Microlab, Inc. (Norcross, GA) and were reported to be within 0.4% of calculated values. Flash column chromatography was performed using silica gel (230−400 mesh). Synthesis of compounds **1**−**3** was carried out as previously described,[19] and the two series of compounds: **4**, **5**, **7**−**9**, and **6**, **10**−**12**, were synthesized according to the general scheme described in Figure 1B, which illustrates the synthesis of compound **4** as example.

Succinic Acid Mono-[2-(4,8-dimethyl-non-1-enyl)-2,5,7,8-tetramethyl-chroman-6-yl] Ester (4): Step a. A solution of 6-hydroxy-2,5,7,8-tetramethyl-chroman-2-carboxylic acid methyl ester (**i**, 41.9 mmol), *t*-butyl-dimethyl-silyloxy chloride (62.8 mmol), and imidazole (172.2 mmol) in 100 mL of DMF was stirred at 85−95 °C for 16 h and cooled to room temperature. The solution was diluted with 200 mL of ethyl acetate, washed, in tandem, with H_2O, 1% HCl, saturated $NaHCO_3$, and brine, dried with Na_2SO_4, and concentrated. Purification by flash silica gel chromatography gave the product, 6-(*t*-butyl-dimethyl-silyloxy)-2,5,7,8-tetramethyl-chroman-2-carboxylic acid methyl ester (**ii**) as white solid in 99% yield. ^{1}H NMR (300 MHz, $CDCl_3$) δ 0.11(s, 6H), 1.04 (s, 9H), 1.62 (s, 3H), 1.76−1.86(m, 1H), 2.01(s, 3H), 2.11(s, 3H), 2.16 (s, 3H), 2.22−2.30 (m, 1H), 3.49−3.65 (m, 2H), 3.69(s, 3H), 4.22 (s, 1H).

Step b. To a stirring solution of compound **ii** (15 g, 39.7 mmol) in 150 mL of dry hexane at −60 °C was added 40 mL of 1 M diisobutyl aluminum hydride (DIBAL-H) in hexane dropwise over a period of 90 min. The solution was stirred in ice bath for 1 h, and 100 mL of methanol followed by 75 mL of H_2O was added to the solution to quench the reaction. The mixture was extracted with 90 mL of ethyl acetate/hexane (1:2) three times, and the pooled organic phase was dried and concentrated. The residue was purified by chromatography, resulting in 6-(*t*-butyl-dimethyl-silyloxy)-2,5,7,8-tetramethyl-chroman-2-carbaldehyde (**iii**) as white solid in 88% yield. ^{1}H NMR (300 MHz, $CDCl_3$) δ 0.11 (s, 6H), 1.04 (s, 9H), 1.39 (s, 3H), 1.76−1.86 (m, 1H), 2.01 (s, 3H), 2.11 (s, 3H), 2.16 (s, 3H), 2.22−2.30 (m, 1H), 3.49−3.65 (m, 2H), 9.62 (s, 1H).

Step c. To a suspension of 1-bromo-3.7-dimethyl octanyl phosphonium (1.05 mmol) in 20 mL of anhydrous THF at 0 °C was added 1.05 mL of 1 M lithium bis(trimethysilyl)amide in THF. The mixture was stirred at 0 °C for 30 min, and compound **iii** (1 mmol) in 10 mL of THF was slowly added over a period of 1 h. After being stirred at room temperature for 1 h, the solution was concentrated, diluted with 20 mL of ethyl acetate, and washed, in tandem, with H_2O and brine. The residue was purified by flash silica gel chromatography to afford *t*-butyl-[2-(4,8-dimethyl-non-1-enyl)-2,5,7,8-tetramethyl-chroman-6-yloxy]-dimethylsilane (**iv**) as colorless oil in 80% yield. ^{1}H NMR (300 MHz, $CDCl_3$) δ 0.11 (s, 6H), 0.86−0.95 (m, 6H), 1.04 (s, 9H), 1.39 (s, 1H), 1.49−1.56 (m, 1H), 1.76−1.86 (m, 1H), 2.01−2.06 (m, 2H), 2.11 (s, 3H), 2.17 (s, 6H), 2.25−2.32 (m, 1H), 2.62 (t, J = 6.60 Hz, 2H), 5.30−5.44 (m, 2H).

Step d. A solution of compound **iv** (0.67 mmol) in anhydrous THF (10 mL) was cooled to 0 °C, to which was added 0.3 mL of 1 M TBAF (tetrabutyl ammonium fluoride) in THF. After being stirred at 0 °C for 1 h, the solution was concentrated, diluted with ethyl acetate (20 mL), washed with water and brine, and dried. Purification of the residue by flash silica gel chromatography gave 2-(4,8-dimethyl-non-1-enyl)-2,5,7,8-tetramethyl-chroman-6-ol (**v**) as colorless syrup in 96% yield. ^{1}H NMR (300 MHz, $CDCl_3$) δ): 0.86−0.95 (m, 9H), 1.39 (s, 1H), 0.98−1.56 (m, 11H), 1.76−1.86 (m, 1H), 2.01−232 (m, 12H), 2.62 (t, J = 6.60 Hz, 2H), 4.20 (s, 1H), 5.31−5.42 (m, 2H).

Step e. A mixture of compound **v** (0.58 mmol), succinic anhydrate (1.16 mmol), and pyridine (93 μL) in dry CH_2Cl_2 (15 mL) was stirred at refluxing temperature for 16 h. The solution was cooled to room temperature, concentrated, and purified by flash silica gel chromatography to give compound **4** as white solid in 88% yield. ^{1}H NMR (300 MHz, $CDCl_3$) δ 0.75−0.90 (m, 9H), 1.00−1.58 (m, 12H), 1.68−1.82 (m, 2H), 1.96 (s, 3H), 2.01 (s, 3H), 2.06−2.28 (m, 4H), 2.30−2.40 (m, 1H), 2.58 (t, J = 5.94 Hz, 2H), 2.83 (t, J = 6.42 Hz, 2H), 2.94 (t, J = 5.49 Hz, 2H), 5.31−5.38 (m, 2H). HRMS exact mass of $C_{28}H_{42}O_5$ $(M + Na)^+$, 481.2930 amu; observed mass of (M + Na)+, 481.2947 amu. Anal. calcd C 73.33, H 9.23, O 17.44; found C 73.49, H 9.46, O 17.56.

General Procedure for Preparing Ether-Linked Alkanoic Acid Derivatives of Compound v (Step f). A mixture of compound **v** (0.58 mmol) and NaH (0.64 mmol) in anhydrous DMF (5 mL) was stirred at 0 °C for 30 min, to which bromoalkanoic acid methyl ester (1.16 mmol) in DMF (1 mL) was added. After being stirred at room temperature for 16 h, the reaction mixture was diluted with ethyl acetate, washed with water and brine, dried, and concentrated. The crude residue was treated with 1 N NaOH in methanol for 3 h. The solution was neutralized with 1N HCl aqueous solution, concentrated, diluted with ethyl acetate, washed with water and brine, dried, and concentrated. Purification of the residue by flash column chromatography gave compounds **5**, and **7**−**9** as white solid in 70−78% yield.

[2-(4,8-Dimethyl-non-1-enyl)-2,5,7,8-tetramethyl-chroman-6-yloxy]-acetic Acid (5). ^{1}H NMR (300 MHz, $CDCl_3$) δ 0.64−0.87 (m, 9H), 0.94−1.56 (m, 11H), 1.70−1.83 (m, 1H), 1.89−2.06 (m, 2H), 2.10−2.34 (m, 10H), 2.48−2.63 (m, 2H), 4.35 (s, 2H), 5.41 (d, J = 18.75 Hz, 2H). 4.35 (s, 2H), 2.63−2.48(m, 2H), 2.34−2.10(m, 10H), 2.06−1.89 (m, 2H), 1.83−1.70 (m, 1H), 1.56−0.94 (m, 11H), 0.87−0.64 (m, 9H). HRMS exact mass of $C_{26}H_{40}O_4$ $(M + Na)^+$, 439.2824 amu; observed mass of $(M + Na)^+$, 439.2840 amu. Anal. calcd C 74.96, H 9.68, O 15.36; found C 75.13, H 9.77, O 15.47.

3-[2-(4,8-Dimethyl-non-1-enyl)-2,5,7,8-tetramethyl-chroman-6-yloxy]-propionic Acid (7). ^{1}H NMR (300 MHz, $CDCl_3$) δ 0.65−0.85 (m, 9H), 1.04−1.56 (m, 12H), 1.74−1.81 (m, 1H), 1.90−2.41 (m, 13H), 2.54 (t, J = 6.75 Hz), 2.80 (t, J = 6.36 Hz, 2H), 3.99 (t, J = 6.3 Hz, 2H), 5. 40 (d, J = 18.75 Hz, 2H). HRMS exact mass of $C_{27}H_{42}O_4$ $(M + Na)^+$, 453.2981 amu; observed mass of $(M + Na)^+$, 453.3013 amu. Anal. calcd C 75.31, H 9.83, O 14.86; found C 75.23, H 9.87, O 14.67.

4- [2-(4,8-Dimethyl-non-1-enyl)-2,5,7,8-tetramethyl-chroman-6-yloxy]-butyric Acid (8). ^{1}H NMR (300 MHz, $CDCl_3$) δ 0.68−0.90 (m, 9H), 1.04−1.56 (m, 17H), 1.74−1.81 (m, 1H), 1.90−2.07 (m, 2H), 2.09−2.40 (m, 12H), 2.58 (t, J = 5.88 Hz, 2H), 2.69 (t, J = 7.40 Hz, 2H), 3.70 (t, J = 6.0 Hz, 2H), 5.37−5.44 (m, 2H). HRMS exact mass of $C_{28}H_{44}O_4$ $(M + Na)^+$, 467.3138 amu; observed mass of $(M + Na)^+$, 467.3161 amu. Anal. calcd C 75.63, H 9.97, O 14.39; found C 75.58, H 9.89, O 14.33.

5- [2-(4,8-Dimethyl-non-1-enyl)-2,5,7,8-tetramethyl-chroman-6-yloxy]-pentanoic Acid (9). ^{1}H NMR (300 MHz, $CDCl_3$) δ 0.69−0.89 (m, 9H), 0.99−1.57 (m, 14H), 1.74−2.05 (m, 6H), 2.09 (s, 3H), 2.13 (s, 3H), 2.17 (s, 3H), 2.24−2.40 (m, 1H), 2.48 (t, J = 6.69 Hz, 2H), 2.57 (t, J = 5.91 Hz, 2H), 3.66 (t, J = 5.76 Hz, 2H), 5.36−5.43 (m, 2H). HRMS exact mass of $C_{29}H_{46}O_4$ $(M + Na)^+$, 481.3294 amu; observed mass of $(M + Na)^+$, 481.3314 amu. Anal. calcd C 75.94, H 10.11, O 13.95; found C 75.83, H 10.06, O 13.92.

General Procedure for Hydrogenolysis (Step g). A mixture of the α,β-unsaturated acid (compounds **5** and **7**− **9**; 0.37 mmol), 10% Pd/C (20 mg) in ethyl acetate was shaken under H_2 at 56 psi for 16 h, filtered, and concentrated. Purification of the residue by flash silica gel column gave compounds **6** and **10**−**12** as white solid in quantitative yield.

[2-(4,8-Dimethyl-nonyl)-2,5,7,8-tetramethyl-chroman-6-yloxy]-acetic Acid (6). ^{1}H NMR (300 MHz, $CDCl_3$) δ 0.86 (dd, J = 6.57, 6.09 Hz, 9H), 1.03−1.61 (m, 19H), 1.74−1.86 (m, 2H), 2.09 (s, 3H), 2.14 (s, 3H), 2.18 (s, 3H), 2.58 (t, J = 6.69 Hz, 2H), 4.36 (s, 2H). HRMS exact mass of $C_{26}H_{42}O_4$ $(M + Na)^+$, 441.2981 amu; observed mass of $C_{26}H_{42}O_4$ $(M + Na)^+$, 441.3000 amu. Anal. calcd C 74.60, H 10.11, O 15.29; found C 74.46, H 10.31, O 15.40.

3- [2-(4,8-Dimethyl-nonyl)-2,5,7,8-tetramethyl-chroman-6-yloxy]-propionic Acid (10). ^{1}H NMR (300 MHz, $CDCl_3$) δ 0.83 (dd, J = 5.22, 5.09 Hz, 9H), 0.99−1.56 (m, 18H), 1.69−1.81 (m, 2H), 2.05 (s, 3H), 2.10 (s, 3H), 2.14 (s, 3H), 2.53 (t, J = 6.75 Hz; 2H), 2.80 (t, J = 6.36 Hz, 2H), 3.92 (t, J = 6.33 Hz, 2H). HRMS exact mass of $C_{27}H_{44}O_4$ $(M + Na)^+$, 455.3138 amu; observed mass of $C_{27}H_{44}O_4$ $(M + Na)^+$, 455.3152 amu. Anal. calcd C 74.96, H 10.25, O 14.79; found C 74.83, H 10.19, O 14.67.

4- [2-(4,8-Dimethyl-nonyl)-2,5,7,8-tetramethyl-chroman-6-yloxy]-butyric Acid (11). ^{1}H NMR (300 MHz, $CDCl_3$) δ 0.86 (dd, J = 5.01, 5.84 Hz, 9H), 1.03−1.63 (m, 18H), 1.71−1.88 (m, 2H), 2.09−2.17 (m, 11H), 2.58 (t, J = 6.49 Hz, 2H), 2.68 (t, J = 7.42 Hz, 2H), 3.70 (t, J = 5.98 Hz, 2H). HRMS exact mass of $C_{28}H_{46}O_4$ $(M + Na)^+$, 469.3294 amu; observed mass of $C_{28}H_{46}O_4$ $(M + Na)^+$, 469.3321 amu. Anal. calcd C 75.29, H 10.38, O 14.33; found C 75.35, H 10.30, O 14.46.

5-[2-(4,8-Dimethyl-nonyl)-2,5,7,8-tetramethyl-chroman-6-yloxy]-pentanoic Acid (12). ^{1}H NMR (300 MHz, $CDCl_3$) δ 0.86 (dd, J = 5.13, 5.96 Hz, 9H), 1.05−1.62 (m, 18H), 1.70−1.88 (m, 6H), 2.09 (s, 3H), 2.13 (s, 3H), 2.17 (s, 3H), 2.48 (t, J = 7.05 Hz, 2H), 2.57 (t, J = 6.81 Hz, 2H), 3.66 (t, J = 5.92 Hz, 2H). HRMS exact mass of $C_{29}H_{48}O_4$ $(M + Na)^+$, 483.3451 amu; observed mass of $C_{29}H_{48}O_4$ $(M + Na)^+$, 483.3472 amu. Anal. calcd C 75.61, H 10.50, O 13.89; found C 75.75, H 10.66, O 13.91.

Cells and Cell Culture. 4T1 murine and MCF-7 and SKBR3 human breast cancer cells were purchased from American Type Culture Collection (Manassas, VA) and cultured in RPMI 1640 or DEME/F12 medium supplemented with penicillin−streptomycin and 10% fetal bovine serum (Invitrogen, Carlsbad, CA). MCF-10A nonmalignant breast epithelial cells were kindly provided by Professor Robert Brueggemeier (The Ohio State University) and maintained in the same medium supplemented with 5% FBS, 100 U of penicillin, 100 g/mL streptomycin, 20 ng/mL epidermal growth factor, 10 ng/mL insulin, 100 ng/mL cholera toxin, and 500 ng/mL hydrocortisone. All cell types were cultured at 37 °C in a humidified incubator containing 5% CO_2.

Adhesion Assay. Ninety-six-well plates were coated with 12% (v/v) Matrigel (BD Biosciences), 2 μg/mL vitronectin (Invitrogen), 10 μg/mL collagen IV (Sigma-Aldrich), 10 μg/mL fibronectin (Calbiochem), or 10 μg/mL laminin (Invitrogen) at 37 °C for 1 h and washed twice with washing buffer (0.1% BSA-containing RPMI medium) followed by blocking with 0.5% BSA-containing RPMI medium at 37 °C for 60 min. 4T1 cells were treated with individual derivatives at the indicated concentrations at 37 °C in a CO_2 incubator for 60 min, and 2×10^4 cells in 100 μL were seeded in each well. Cells were allowed to adhere to the Matrigel-coated surface for 30 min at 37 °C, and nonadherent cells were removed by gentle washing with the aforementioned washing buffer. Adherent cells were fixed with 10% formalin, stained with 0.5% crystal violet, and dissolved in 2% SDS. Absorbance at 570 nm was measured in an ELISA plate reader (Molecular Devices, Sunnyvale, CA).

Migration Assay. 4T1 cells were trypsinized for 5 min, washed, and suspended in 0.2% FBS-supplemented RPMI 1640 medium. Cells (5×10^4) in 0.5 mL of 0.2% FBS-supplemented RPMI medium containing individual test agents at the indicated concentrations were added to the upper chamber (i.e., insert) of each Transwell system (12 mm, polycarbonate, 12 μm pore, Millipore) in a 24-well plate and incubated at 37 °C in a CO_2 incubator for 30 min. The inserts were then switched to a new well containing 10% FBS-supplemented RPMI 1640 medium for 24 h. All cells in each well were fixed with 10% formalin, followed by staining with 0.5% crystal violet. To quantify migrated cells, cells attached to the bottom side of the upper chamber and in the bottom of the well were wiped with a moistened cotton swab, which was then rinsed with 80 μL of double distilled water (DDW). The cells were then dissolved by the addition of 320 μL of 100% methanol. Enumeration of nonmigrated cells was done by placing the chamber into 400 μL of 80% methanol and incubating for 30 min in an orbital shaker. Absorbance at 570 nm was measured in an ELISA plate reader. Percentage of cell migration in each well was calculated using the following equation: % of migration = 100[(optical density (OD) of migrated cells) − (OD of background)]/([(OD of migrated cells) − (OD of background)] + [(OD of nonmigrated cells) − (OD of background)]). The migration activity in each

treatment group is expressed as a percentage of that in the vehicle controls, which was considered to be 100%.

F-Actin Immunostaining. To assess the effect of test compounds on actin cytoskeletal structures, cells were seeded onto coverslips in six-well plates and incubated overnight, followed by exposure to individual agents at the indicated concentrations for 4 h in 2% FBS-containing RPMI 1640 medium. Cells were then fixed in 3.7% formaldehyde, permeabilized with PBS containing 0.1% Triton X-100 and 0.1% BSA for 1 h, and then incubated with Alexa Fluor 488 phallotoxin staining solution (Molecular Probes, Inc., Eugene, OR) for 30 min. Nuclear counterstaining was achieved by use of 4,6-diamidino-2-phenylindole (DAPI)-containing mounting medium. Immuno-cytochemically labeled cells were visualized and images captured using a Zeiss microscope (LSM510) with Ar and HeNe lasers, appropriate filters (excitation wavelengths were 488 and 543 nm), and a 63 × 1.4 numerical aperture water immersion lens. Differences in fluorescence intensity were calculated from comparisons of the control sample with each of the treatment samples under the same threshold using MacBiophotonic ImageJ software (National Institutes of Health) and were expressed as percentages of the fluorescent intensity of the untreated control. Statistical significance was evaluated using Student's *t* test and considered significant at $P < 0.05$.

Cell Viability Assay. Cell viability was assessed by using the 3-(4,5-dimethylthiazol-2-yl)-2,5-diphenyl-2*H*-tetrazolium bromide (MTT) assay in six replicates in 96-well plates. The 4T1 cells were seeded at 6000 cells per well in 10% FBS-supplemented RPMI 1640 for 24 h, followed by treatments with various compounds in 2% FBS-supplemented RPMI 1640 at the indicated concentrations. Controls received DMSO at a concentration equal to that in drug-treated cells. After the end of incubation, MTT (0.5 mg/mL) in 10% FBS-supplemented RPMI 1640 was added to each well and cells were incubated at 37 °C for 2 h. Medium was removed, and the reduced MTT dye was solubilized in DMSO (200 μL/well). Absorbance was determined at 570 nm by a 96-well plate reader.

Statistical Analysis. The GraphPad InStat software V3.0 was used to perform all data analysis. *P* values were generated using the Dunnett Test for multiple comparisons to one control. Differences were considered significant at $P < 0.05$.

Acknowledgment. This work is supported by National Institutes of Health, grant CA12250, and the Lucius A. Wing Endowed Chair Fund at The Ohio State University.

References

(1) Neuzil, J.; Tomasetti, M.; Zhao, Y.; Dong, L. F.; Birringer, M.; Wang, X. F.; Low, P.; Wu, K.; Salvatore, B. A.; Ralph, S. J. Vitamin E analogs, a novel group of "mitocans," as anticancer agents: the importance of being redox-silent. *Mol. Pharmacol.* **2007**, *71*, 1185–1199.

(2) Wang, X. F.; Dong, L.; Zhao, Y.; Tomasetti, M.; Wu, K.; Neuzil, J. Vitamin E analogues as anticancer agents: lessons from studies with alpha-tocopheryl succinate. *Mol. Nutr. Food Res.* **2006**, *50*, 675–685.

(3) Crispen, P. L.; Uzzo, R. G.; Golovine, K.; Makhov, P.; Pollack, A.; Horwitz, E. M.; Greenberg, R. E.; Kolenko, V. M. Vitamin E succinate inhibits NF-kappaB and prevents the development of a metastatic phenotype in prostate cancer cells: implications for chemoprevention. *Prostate* **2007**, *67*, 582–590.

(4) Hahn, T.; Szabo, L.; Gold, M.; Ramanathapuram, L.; Hurley, L. H.; Akporiaye, E. T. Dietary administration of the proapoptotic vitamin E analogue alpha-tocopheryloxyacetic acid inhibits metastatic murine breast cancer. *Cancer Res.* **2006**, *66*, 9374–9378.

(5) Schmidmaier, R.; Baumann, P. ANTI-ADHESION evolves to a promising therapeutic concept in oncology. *Curr. Med. Chem.* **2008**, *15*, 978–990.

(6) Simmons, D. L. Anti-adhesion therapies. *Curr. Opin. Pharmacol.* **2005**, *5*, 398–404.

(7) Lelekakis, M.; Moseley, J. M.; Martin, T. J.; Hards, D.; Williams, E.; Ho, P.; Lowen, D.; Javni, J.; Miller, F. R.; Slavin, J.; Anderson, R. L. A novel orthotopic model of breast cancer metastasis to bone. *Clin. Exp. Metastasis* **1999**, *17*, 163–170.

(8) Yoneda, T.; Michigami, T.; Yi, B.; Williams, P. J.; Niewolna, M.; Hiraga, T. Actions of bisphosphonate on bone metastasis in animal models of breast carcinoma. *Cancer* **2000**, *88*, 2979–2988.

(9) Tao, K.; Fang, M.; Alroy, J.; Sahagian, G. G. Imagable 4T1 model for the study of late stage breast cancer. *BMC Cancer* **2008**, *8*, 228.

(10) McLean, G. W.; Carragher, N. O.; Avizienyte, E.; Evans, J.; Brunton, V. G.; Frame, M. C. The role of focal-adhesion kinase in cancer—a new therapeutic opportunity. *Nat. Rev. Cancer* **2005**, *5*, 505–515.

(11) Mitra, S. K.; Hanson, D. A.; Schlaepfer, D. D. Focal adhesion kinase: in command and control of cell motility. *Nat. Rev. Mol. Cell Biol.* **2005**, *6*, 56–68.

(12) Kim, B.; Feldman, E. L. Insulin-like growth factor I prevents mannitol-induced degradation of focal adhesion kinase and Akt. *J. Biol. Chem.* **2002**, *277*, 27393–27400.

(13) Mitra, S. K.; Schlaepfer, D. D. Integrin-regulated FAK-Src signaling in normal and cancer cells. *Curr. Opin. Cell Biol.* **2006**, *18*, 516–523.

(14) Ochel, H. J.; Schulte, T. W.; Nguyen, P.; Trepel, J.; Neckers, L. The benzoquinone ansamycin geldanamycin stimulates proteolytic degradation of focal adhesion kinase. *Mol. Genet. Metab.* **1999**, *66*, 24–30.

(15) Roberts, W. G.; Ung, E.; Whalen, P.; Cooper, B.; Hulford, C.; Autry, C.; Richter, D.; Emerson, E.; Lin, J.; Kath, J.; Coleman, K.; Yao, L.; Martinez-Alsina, L.; Lorenzen, M.; Berliner, M.; Luzzio, M.; Patel, N.; Schmitt, E.; LaGreca, S.; Jani, J.; Wessel, M.; Marr, E.; Griffor, M.; Vajdos, F. Antitumor activity and pharmacology of a selective focal adhesion kinase inhibitor, PF-562,271. *Cancer Res.* **2008**, *68*, 1935–1944.

(16) Van Assche, G.; Rutgeerts, P. Physiological basis for novel drug therapies used to treat the inflammatory bowel diseases. I. Immunology and therapeutic potential of antiadhesion molecule therapy in inflammatory bowel disease. *Am. J. Physiol. Gastrointest. Liver Physiol.* **2005**, *288*, G169–174.

(17) Lockwood, C. M.; Elliott, J. D.; Brettman, L.; Hale, G.; Rebello, P.; Frewin, M.; Ringler, D.; Merrill, C.; Waldmann, H. Anti-adhesion molecule therapy as an interventional strategy for autoimmune inflammation. *Clin. Immunol.* **1999**, *93*, 93–106.

(18) Gupta, G. P.; Massague, J. Cancer metastasis: building a framework. *Cell* **2006**, *127*, 679–695.

(19) Shiau, C. W.; Huang, J. W.; Wang, D. S.; Weng, J. R.; Yang, C. C.; Lin, C. H.; Li, C.; Chen, C. S. alpha-Tocopheryl succinate induces apoptosis in prostate cancer cells in part through inhibition of Bcl-xL/Bcl-2 function. *J. Biol. Chem.* **2006**, *281*, 11819–11825.